International Journal of Mass Spectrometry 299 (2011) 94–101

Contents lists available at ScienceDirect

International Journal of Mass Spectrometry

journal homepage: www.elsevier.com/locate/ijms

Direct mass analysis of neutral molecules by superconductivity

Masataka Ohkubo[a,*], Shigetomo Shiki[a], Masahiro Ukibe[a], Shigeo Tomita[b], Shigeo Hayakawa[c]

[a] National Institute of Advanced Industrial Science and Technology (AIST), Umezono, Tsukuba, Ibaraki 305-8568, Japan
[b] Institute of Applied Physics, University of Tsukuba, Tsukuba, Ibaraki 305-0006, Japan
[c] Department of Chemistry, Graduate School of Science, Osaka Prefecture University, Nakaku, Sakai, Osaka 599-8531, Japan

ARTICLE INFO

Article history:
Received 19 July 2010
Received in revised form
28 September 2010
Accepted 28 September 2010
Available online 7 October 2010

Keywords:
Tandem mass spectrometry
Superconducting detector
Cryodetector
Neutral molecule
Collisionally activated dissociation (CAD)
Electron transfer dissociation (ETD)

ABSTRACT

Dissociation related to ion collision reactions produces neutral fragments in addition to ionic fragments, and the ability to analyze both neutral and ionic fragments is crucial for fully understanding chemical reactions in the gas phase. However, conventional mass spectroscopy (MS) instruments are unable to directly analyze multiple neutral fragments without reionization. This inability is called "*neutral loss*." We report the first tandem MS instrument realized by a kinetic-energy-sensitive cryodetector (a superconducting tunnel junction operated in the Giaever mode) as the second mass separation (KEMS) to quantitatively analyze multiple fragment molecules, either neutral or ionic, in a keV kinetic energy range. The performance of the MS/KEMS instrument was examined using the collisions of singly charged acetone or acetyl precursors with a Xe target. These singly charged ions undergo either collisionally activated dissociation (CAD) or electron transfer dissociation (ETD), including a dissociation path of $ABA^+ + e \rightarrow ABA^* \rightarrow A + B + A$ or AB + A, which produces neutral fragments only. Our approach is able to determine the branching ratios of the competing CAD and ETD processes and may provide a method to overcome the neutral loss.

1. Introduction

Ion collision reactions in the gas phase occur in many situations, including both natural phenomena (interstellar clouds, cometary comae, planetary ionospheres) and artificial phenomena (combustion engines, thin film deposition, fusion reactors). These collisions stimulate our interest in prebiotic organic molecules in space, plasma-aided nanofabrication, and future power supplies [1]. A typical gas phase reaction that produces only neutral product molecules is dissociative ion-electron recombination (DR) for singly charged ions, which has been actively investigated in the fields of atomic and molecular physics and interstellar physical chemistry [2]. In the DR processes, a singly charged ion is neutralized by electron capture and the resultant metastable neutral molecule dissociates into multiple neutral fragments including radicals, which play an important role in succeeding chemical reactions. The high abundance of organic molecules in the giant molecular cloud Sagittarius B2, located near the center of the Milky Way, is one of the mysteries of interstellar physical chemistry [3]. Interstellar organic molecules such as acetone, acetic acid, and formic acid may be formed through DR. Moreover, gas phase reactions are now essential for identifying and analyzing biomolecules. The reactions are expanding from ion/molecule collisions to ion/ion collisions [4], but singly charged precursor ions are difficult to be analyzed because of the neutral loss. Therefore, the study on the neutral fragment analysis is important.

In the field of mass spectrometry (MS), the DR-type reaction is called electron capture dissociation (ECD) [5]. A similar reaction occurs in electron transfer from a target atom or molecule, which is called electron transfer dissociation (ETD) [5]. The gas phase reaction studied in this work is based on either interaction of a singly charged precursor ion with a kinetic energy (E) of a few keV with an electron of the outermost orbit of a target gas or with a practically stationary target gas. If we take a precursor molecule ABA, the processes associated with the electron capture are expressed as follows

$$ABA^+ + e^- \rightarrow ABA^* \rightarrow \begin{cases} ABA^* \\ AB + A \\ AA + B \\ A + B + A. \end{cases} \quad (1)$$

The third reaction is rare because of a high rearrangement energy barrier, so there are four neutral products to be analyzed: the metastable neutral precursor, which is neutralized by electron capture and reaches a molecule detector within its lifetime (ABA^*), and the neutral fragments (A, B, and AB), which are dissociated from ABA^*. To evaluate the dissociation branching ratios, the yields of those neutral products should be quantitatively analyzed; how-

* Corresponding author at: National Institute of Advanced Industrial Science and Technology (AIST), Research Institute of Instrumentation Frontier (RIIF), AIST Tsukuba Central 2, 1-1-1, Umezono, Tsukuba, Ibaraki 305-8568, Japan.
Tel.: +81 29 861 5685; fax: +81 29 861 5730.
E-mail address: m.ohkubo@aist.go.jp (M. Ohkubo).

1387-3806/$ – see front matter © 2010 Elsevier B.V. All rights reserved.
doi:10.1016/j.ijms.2010.09.027

ever, the multiple neutrals cannot be separated by conventional MS using an electromagnetic force and molecule detectors operating at room temperature except Nevatron [6].

Another dissociation reaction called collisionally activated dissociation (CAD) [7] also produces neutral fragments in addition to one ionic fragment, when the precursor ions are singly charged, as is expressed by

$$\mathrm{ABA}^+ + \mathrm{T} \rightarrow \mathrm{ABA}^{+*} \rightarrow \begin{cases} \mathrm{ABA}^{+*} \\ \mathrm{AB}^+ + \mathrm{A} \\ \mathrm{AB} + \mathrm{A}^+ \\ \mathrm{A}^+ + \mathrm{B} + \mathrm{A} \\ \cdots \end{cases} \quad (2)$$

where T is the target atom or molecule. The investigation on singly charged precursor ions, which have the lowest ionization potential, is important because of the prevalence of singly charged ions in gas phase chemical reactions. When we detect only ions, it is impossible to distinguish third and fourth paths in the reaction (2). Furthermore, in some collision systems, ETD and CAD competitively occur, thereby making branching path analysis difficult without a direct analytical method for multiple neutrals.

If all product molecules are neutral, multiple neutrals can be analyzed using huge magnetic synchrotron storage rings for heavy ions, which are operated in a kinetic energy range of MeV and are assisted by kinetic-energy-sensitive silicon particle detectors [8]. The kinetic energy of a precursor ion is distributed among neutral fragments according to their mass values with a small kinetic energy release (KER) of several eV upon dissociation of the metastable neutral molecule. The neutralized precursor ions and neutral fragments escape from the circulation orbit of the ring and are detected by the silicon detector. Mass analysis of the neutral products is performed by measuring the kinetic energies of individual neutral products, instead of the spatial and temporal separations used in the conventional MS. The KER values can be neglected compared with the E values. In the storage ring experiments, branching ratio determination requires a mesh grid technique [9] to distinguish different molecular species, because all product neutrals impinge on the silicon detector surface simultaneously and such multi-impact events create a single output pulse.

The silicon detectors cannot be used for most MS instruments or the recently developed compact electrostatic storage rings [10] of which the precursor ion energy range is in a few tens of keV. This is because the silicon detectors have a surface dead layer of finite thickness, which originates from the detector structure and prevents the penetration of keV particles into the depletion layer [11]. In this situation, no electron–hole pairs are produced and thus results in no output electric pulses. Furthermore, the energy resolution for 12 keV He ions is only 5.4 keV [12], which cannot be used to separate multiple fragments in the keV range. Therefore, kinetic-energy-sensitive detectors which have a high energy resolution and cover a keV range are required [2].

The MeV storage ring method provides information only on *neutral molecules*. In contrast, conventional MS instruments operating in the ~keV range can analyze only *ionic molecules* according to mass/unit-charge (m/z) ratios. Therefore, in ETD, precursor ions should be multiply charged so that one of the fragments produced from a metastable ion with the reduced ionic state has a charge. Although neutralization reionization mass spectroscopy (NRMS) [14] or charge inversion mass spectroscopy (CIMS) [15] can shed light on neutral fragments, they require reionization processes which may lead to additional fragmentation and mask initial quantitative information on the product molecules [14]. No instrument capable of quantitatively analyzing both ionic and neutral fragments produced by the competitive processes of CAD and ETD has been reported up to now.

In this study, we employed a cryodetector for fragment analysis and demonstrated that a tandem MS instrument equipped with a superconducting tunnel junction (STJ) detector overcomes the limitations of both the huge heavy ion storage rings (MeV neutral analysis only) and the conventional MS instruments (keV ion analysis only). We report the instrumentation development and the detailed data analysis presented in Ref. [16]. The developed tandem MS/KEMS instrument can effectively analyze both neutrals and ions at the single-molecule counting mode, and thus can be used to determine the branching ratios of the complex dissociation channels associated with the competing CAD and ETD processes in the keV range.

2. Methods

2.1. Kinetic-energy-sensitive mass spectroscopy (KEMS) with superconducting tunnel junction (STJ)

Superconductivity has provided a class of solid-state particle detectors that are capable of measuring the E values of ~keV particles through a phonon detection scheme [17]. The Cooper-pair breaking by the phonons created by a particle impact event results in an increase of quasiparticle tunneling current through the tunneling barrier of an STJ in the Giaever mode [18]. Application of this detection scheme to MS was first reported on lysozyme detection [19], and simultaneous measurements of time-of-flight (TOF) and charge state were proposed [20]. There was a comprehensive review about the cryogenic detectors before 1999 [21].

In this study, we fabricated the STJ detectors at our institute with photolithographic microprocessing [22] that allowed us to obtain a small pixel size (a few 100 μm), which is favorable for the detection of individual molecules without the multi-particle impacts that occur in large single-pixel detectors. Although an STJ detector chip has one-hundred pixels, one of the STJ pixels was used in this demonstration study. Imaging analysis of product molecules or coincidence analysis between the positions and kinetic energies of product molecules is promising.

The STJ detectors and a few other types of superconducting cryodetectors have been attached to MS instruments for the last decade, especially for the purpose of detecting high-mass molecules such as macroglobulin, immunoglobulin, polystyrene, and viral capsids [19–25]. This trend has evolved because the superconducting detectors have in principle a 100% detection efficiency independent of mass. In addition to detecting large molecules, the superconducting detectors can discriminate different charge states using the kinetic energy measurement for individual ion impacts because the value of E is in principle proportional to the number of unit charge (z) when ions are accelerated in a certain electric field. An ion yield of $^{14}N_2{}^{2+}$ was extracted from a peak at a m/z value of 14 by discriminating different charge states: the peak (m/z 14) is dominated by a large yield of $^{14}N^+$ [26]. This separation using the E measurement is also useful for analyzing multiple neutral fragments, since it is valid for either neutral or ionic fragments. There is a report for measuring ionic or neutral fragments due to scattering with residual gas [27] and a presentation for post-source decay (PSD) [28,29] using superconducting junction molecule detectors for TOF MS with matrix-assisted laser desorption ionization (MALDI).

For this study, a collision cell was added to our earlier instrument [26] with a double-focusing mass spectrometer (JEOL JMS-600W with Nier–Johnson geometry). The slit width of the electrostatic sector affects the kinetic energy distribution of precursor ions. At a current slit setting, the distribution is estimated to be about 30 eV, which is negligibly smaller than the kinetic energy resolution (216–430 eV) of the STJ detector. In front of the STJ detector, an electrostatic ion deflector can select either ionic and neutral molecules

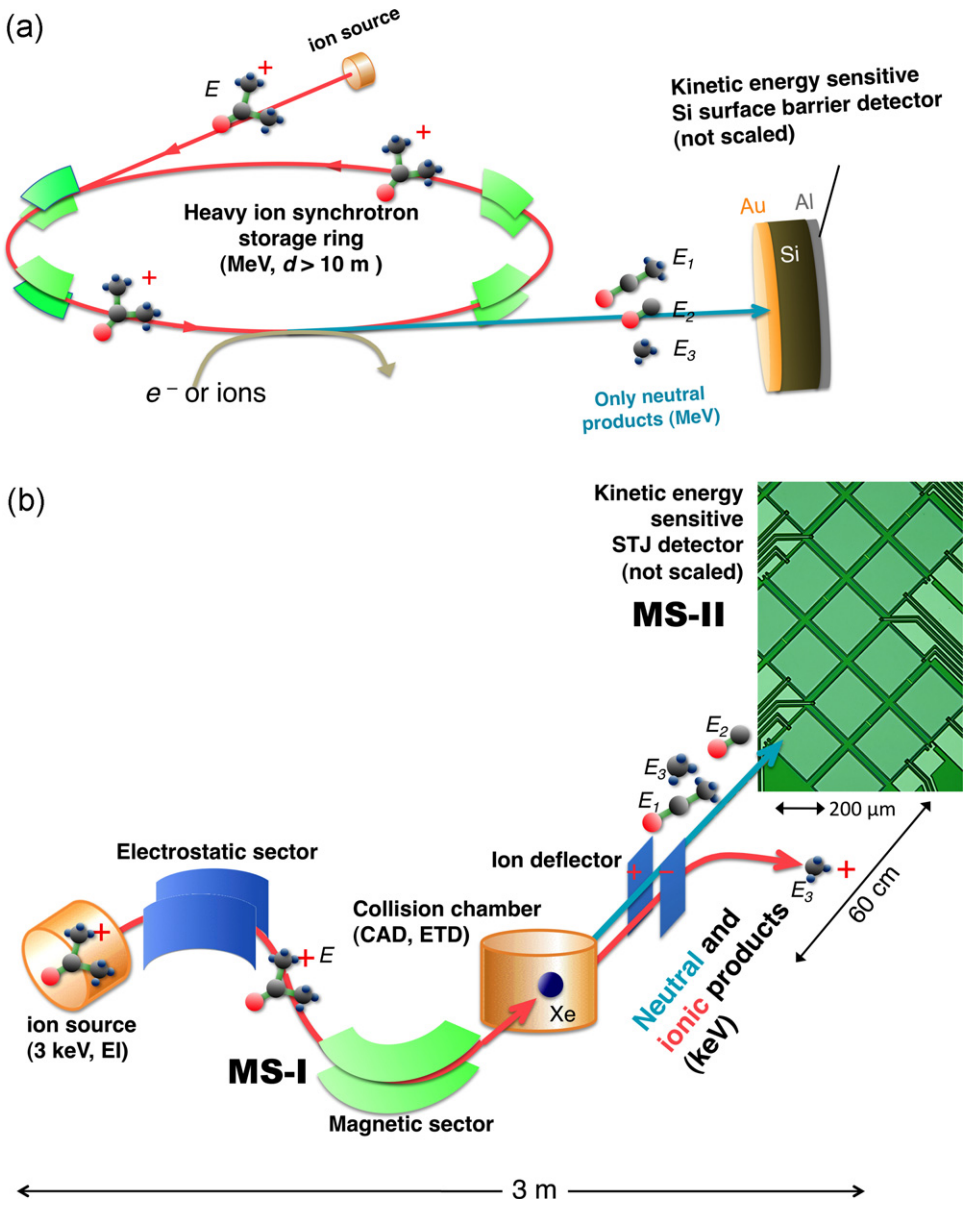

Fig. 1. Comparison between two MS instruments using kinetic energy separation of product molecules. The kinetic energy of the precursor ion is distributed into the fragments according to their mass values: $E = E_1 + E_2 + E_3$. (a) Synchrotron-storage-ring-based MS at MeV range only for neutral molecules. The neutral fragments deviate from the synchrotron orbit and fly toward the Si detector, which can differentiate among multiple neutral molecules at the MeV range. All fragments impinge on the detector's surface simultaneously, so that a mesh technique is required to obtain individual molecular yields. (b) Superconducting compact MS, built as part of this study for keV neutral and ionic molecules. Each fragment deviates slightly according to kinetic energy release upon dissociation; therefore, simultaneous impacts of multiple fragments on a single pixel are almost impossible. One of the STJ pixels in the array detector was used in this study.

or only neutral molecules. The same arrangement was also adapted in Ref. [28] for biomolecules. By comparing two spectra taken by activating and deactivating the ion deflection, one can obtain the fractions of neutral products. An infrared reflection filter that transmits molecules was set on a 4 K stage in front of the STJ detector to avoid room-temperature black-body radiation from the ion source side, which led to the improvement of kinetic energy resolution by avoiding noise due to infrared photons [30].

2.2. Tandem MS/KEMS experiments

Fig. 1 illustrates the difference between the synchrotron-based method and our method. Our instrument that operates at 3 keV is compact compared to the accelerator that occupies a building and operates at MeV. The MS/KEMS instrument consists of a double-focusing MS, an STJ detector operating at 0.3 K, and an ion deflector. The distance between the ion deflector, which is placed 20-cm downstream of the collision cell, and the STJ detector was 60 cm.

The acetone molecules were ionized by electron impact (EI) at 70 eV and accelerated by a voltage of 3 kV. The double-focusing mass spectrometer selected the precursor ions, either acetone radical ions $(CH_3)_2CO^{+\bullet}$ ($m/z = 58$) or acetyl ions CH_3CO^+ ($m/z = 43$) that are the fragments created by the EI ionization. The precursor ions passed through the collision cell causing a part of them to dissociate. When the Xe gas was introduced into the collision cell, the reduction of the precursor ion flux was kept at less than 20% to maintain a single-collision condition. The collisions with a neutral Xe atom can induce both collisional activation and charge-exchange neutralization [31]. A high charge-exchange neutralization efficiency is expected in Xe [32,33]. This predicts a

considerably large competitiveness between CAD and ETD. The competitive CAD–ETD of singly charged precursor ions is very difficult to study using conventional tandem MS instruments.

The energies of the precursor molecule ions, neutralized precursor molecules, product ions, and product neutrals were measured by two STJ detectors with different sizes (100 μm and 200 μm) and structures. The MS/KEMS spectra that plot molecular yield histograms against the kinetic energy axis were recorded for 100–1000 s by deactivating or activating the electrostatic ion deflector at 1 kV. Discrimination between CAD and ETD can be performed through dissociation channel analysis by comparing the (ions + neutrals) and (neutrals only) spectra. The current KEMS instrument has a mass resolution of 5–10 on the kinetic energy axis. Although the mass resolution makes the separation of minor molecular peaks (CH_2CO^+, HCO^+, CH_2^+, CH^+, C^+, etc.) difficult, it suffices to analyze the major reaction channels for ETD and CAD expressed in the reactions (1) and (2). The energy resolution should be improved in the future by modifying the detector design. As per our observations, small junctions have better energy resolution. However, to use a small junction, we require solving a fabrication problem of how to decrease an area of the SiO_2 insulating passivation layer that covers the junction edge and causes an undesirable artifact peak; this will be discussed later.

It has been reported that acetone ions created by EI at 70 eV have a keto structure and ~10% of these acetone are in the first electronically excited A state. The A-state acetone radical ions are known to be an extremely long-lived species and survive for >30 μs prior to the dissociation [34]. The radiative lifetime of the A-state was reported to be from 4 to 14 ms [35], which is negligibly longer than a total flight time of 25 μs in the present experimental setup. The dissociation from the A-state is prompted by a low energy collision that induces an efficient electronic-to-translational energy conversion. In our experimental data without the Xe target, the fraction of the CH_3 neutral, which is recognizable and presumed to be a product of the spontaneous dissociation of $(CH_3)_2CO^{+\bullet}(A) \rightarrow CH_3CO^+ + CH^{3\bullet}$, was only 0.08% of the precursor acetone yield. This small dissociation fraction corresponds to a time constant for the spontaneous dissociation in the order of ms. Consequently, the spontaneous dissociation of the ions that are initially excited to the A state by the EI is negligible in this study.

3. Results

3.1. Kinetic-energy mass analysis (KEMS)

In the course of the detector development for the neutral fragment analyses, the high sensitivity for phonons resulted in an unexpected artifact peak in addition to the main peak. As shown in Fig. 2 (a), the response of the 100-μm-square STJ to 3 keV acetyl ions CH_3CO^+ formed double peaks instead of the desirable single peak in the pulse height spectrum (ion yield vs. kinetic energy). An artifact peak at the lower kinetic energy side was unremarkable for several-tens-kDa macromolecules such as albumin and immunoglobulin G [11,29]. The peak was greatly enhanced for low-mass molecules. It is suggested that the molecule impact at the high kinetic energy per nucleus is related to the double peak formation.

Fig. 3(a) shows a photograph of the STJ detector used to acquire the data in Fig. 2(a) and the cross-sectional structure. Because the ion beam size was over 1 mm, it was assumed that the entire area of the detector structure was uniformly irradiated with the molecules. The trajectory of the fragments was slightly but surely beyond the STJ size deviated by KER [36], and thus no simultaneous impact occurred on the multiple fragments produced by a single collision, unlike the heavy ion synchrotron experiment with the semiconducting detector. The ion counting rates were kept below 3 kcounts/s (cps), which is far below a counting rate at which pulse pile-up occurs (~30 kcps). Therefore, the double peak formation certainly represents the response function to single ion impacts.

The top superconducting electrode had a Nb(200 nm)/Al(50 nm) bilayer structure in order to increase the current output signal by multiple quasiparticle tunneling (Gray effect) [37]. The 700-nm-thick insulating SiO_2 layer was necessary for insulating the top electrode lead and the bottom electrode and for passivating the junction edge. The SiO_2 layer covered the top electrode near the junction edge forming a 6-μm-wide frame at a ratio of 32% between the SiO_2 frame and the exposed Nb surface. The artifact peak had a relative intensity of 32% to the main peak. In addition, a 200-μm-square junction with a SiO_2 frame ratio of 13% exhibited an artifact peak intensity of 12%. These results demonstrate that the artifact peak formation is definitely related to the impact events on the SiO_2 frame. Phonon down conversion due to anharmonic decay [38] in the 700-nm-thick amorphous SiO_2 layer may have resulted in less phonons capable of breaking Cooper-pairs, and thus the low pulse height compared with the direct impact on the Nb surface. The fact that the artifact peak was unremarkable for the macromolecule impacts that created low energy phonons due to low kinetic energy per nucleus supports this explanation. When the initial phonon energy is low, it is expected that, by the anharmonic decay, phonon energies are quickly reduced to below a threshold energy for breaking Cooper-pairs in the superconducting electrode.

The above-mentioned artifact peak phenomenon validated the high sensitivity of the STJ detector for molecule impacts. Even if there was a contamination layer of the Nb surface, it was possible to detect the molecules in contrast to the microchannel plates (MCPs) and secondary electron multiplier (SEM) detectors both of which rely on secondary electron emission. Nevertheless, the large artifact peak precluded the use of the STJ detector for neutral fragment analysis because of the possible peak overlap with the artifact peak. To solve this problem, we fabricated a new detector structure: a 200-μm junction size, a 1600-nm-thick SiO_2 layer, and a phonon-down-conversion layer of Al(100 nm)/Nb(50 nm) at the middle of the SiO_2 layer, as shown in Fig. 3(b). The large junction size led to a low SiO_2 frame ratio. The thicker SiO_2 layer with the phonon-down-conversion layer also reduced the number of phonons with over the threshold energy, which propagated and reached the top electrode.

The phonon-down-conversion Nb/Al layer was expected to have a superconducting gap parameter of 0.4 meV, which was smaller than the 0.6 meV of the Nb(200 nm)/Al(50 nm) electrode, because of the superconducting proximity effect [39]. The 0.6 meV is the threshold energy for breaking Cooper-pairs. With the increase in the proximity effect, such as the Al thickness, the gap parameter decreased. The phonons created by the molecule surface impact on the SiO_2 layer were absorbed in the phonon-down-conversion layer and may have been converted to the phonons of 0.4 meV. The 0.4-meV phonons could not break Cooper-pairs in the superconducting electrodes because of the higher threshold value (0.6 meV). We expected these structural modifications to lead to a decrease of the pulse height for the SiO_2 events to electric noise level. Our expectation did not materialize completely, but a less pronounced artifact peak is seen in Fig. 2(b). We employed this 200-μm-square STJ detector for the MS/KEMS experiments, although the energy resolution degraded from 216 eV to 430 eV. Further investigation is necessary for a more precise understanding and a detector structure adjustment.

There are two reasons for the energy resolution degradation as the junction size increased. First, spatial inhomogeneity of current output pulse heights was enhanced, probably because of finite quasiparticle diffusion length [40]. Second, it is generally known that large capacitance, which is proportional to the junction area, causes an electric noise increase. We plan to fabricate a junction

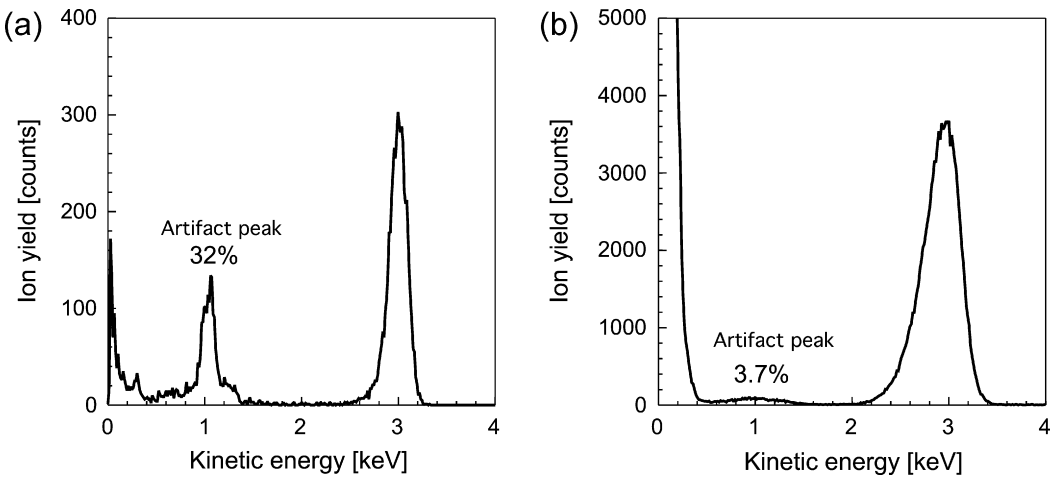

Fig. 2. Response functions (pulse height spectra) to 3 keV CH_3CO^+ ions. (a) 100-μm-square STJ detector. (b) 200-μm-square STJ detector with a thicker SiO_2 layer and a phonon-down-conversion layer (see Fig. 3). Kinetic energy deposited on the detector surface for each single-molecule impact event was measured. Horizontal positions of main peaks in the histograms were calibrated by the kinetic energy of the precursor ions (3 keV). Peaks at the lowest energy side are due to impact events on the electrode leads and electric noise pulses. The corresponding detector structures are shown in Fig. 3. The energy resolution values of the main peaks are (a) 216 eV and (b) 430 eV in full width at half maximum. The unexpected artifact peaks appear around 1 keV.

with a SiO_2 frame area as small as possible, which is a challenge of microfabrication.

3.2. Tandem MS/KEMS analysis

Raw KEMS spectra are shown in Fig. 4(a) for the acetyl precursor, CH_3CO^+, and (b) for the acetone radical precursor, $(CH_3)_2CO^{+\bullet}$. The raw data show the fractions of the product yields relative to the precursor ion yields and the ratios of ions and neutrals. The difference between Figs. 4(a) and (b) is apparent: the fraction of surviving neutralized acetyl radicals relative to the precursor ion yield is almost undetectable (0.04%) in Fig. 4(a), whereas the fraction of the neutralized acetone molecules is as high as 6% in Fig. 4(b). The difference in the neutralization fractions can be understood by considering the enthalpy values (ΔH), $CH_3CO^+ + Xe \rightarrow CH_3CO^{\bullet} + Xe^+$ ($\Delta H = 5.20$ eV), $(CH_3)_2CO^{+\bullet} + Xe \rightarrow (CH_3)_2CO + Xe^+$ ($\Delta H = 2.41$ eV), and dissociative rate constants (to be discussed later). It is reasonable that the reaction channel with the smaller endothermic

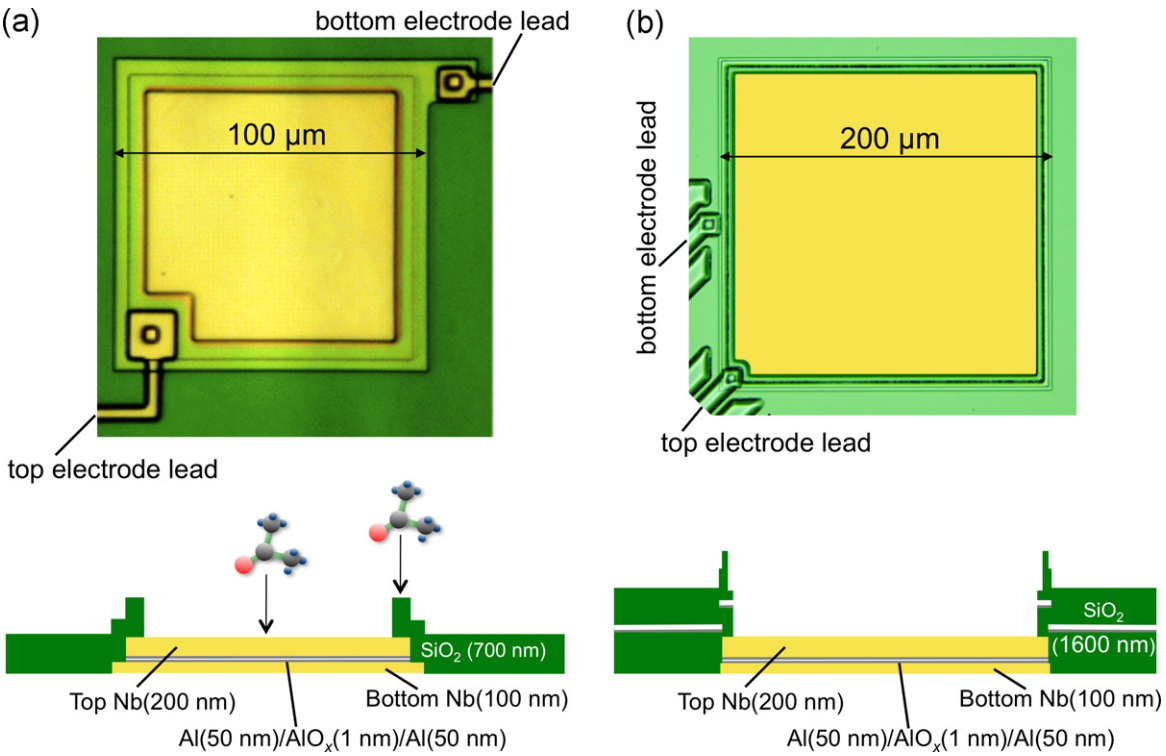

Fig. 3. Top and cross-sectional views of the STJ detectors corresponding to Fig. 2. (a) 100-μm-square STJ. The junction edge is covered by a 700-nm-thick amorphous SiO_2 layer, forming a frame, to insulate the wiring leads for the bottom and top electrodes. The frame area ratio to the naked Nb area in the middle is 32%, which coincides with the relative intensity of the artifact peak. (b) 200-μm-square STJ. The junction edge is covered by a 1.6-μm-thick SiO_2 layer which has a phonon-down-conversion layer [Al(100 nm)/Nb(50 nm), shown by white] in the middle. The frame ratio is 16%. The absorbed phonons in the down conversion layer can have energies less than a superconducting energy gap (2Δ), so that the STJ has no sensitivity and thus reduces the relative intensity of the artifact peak.

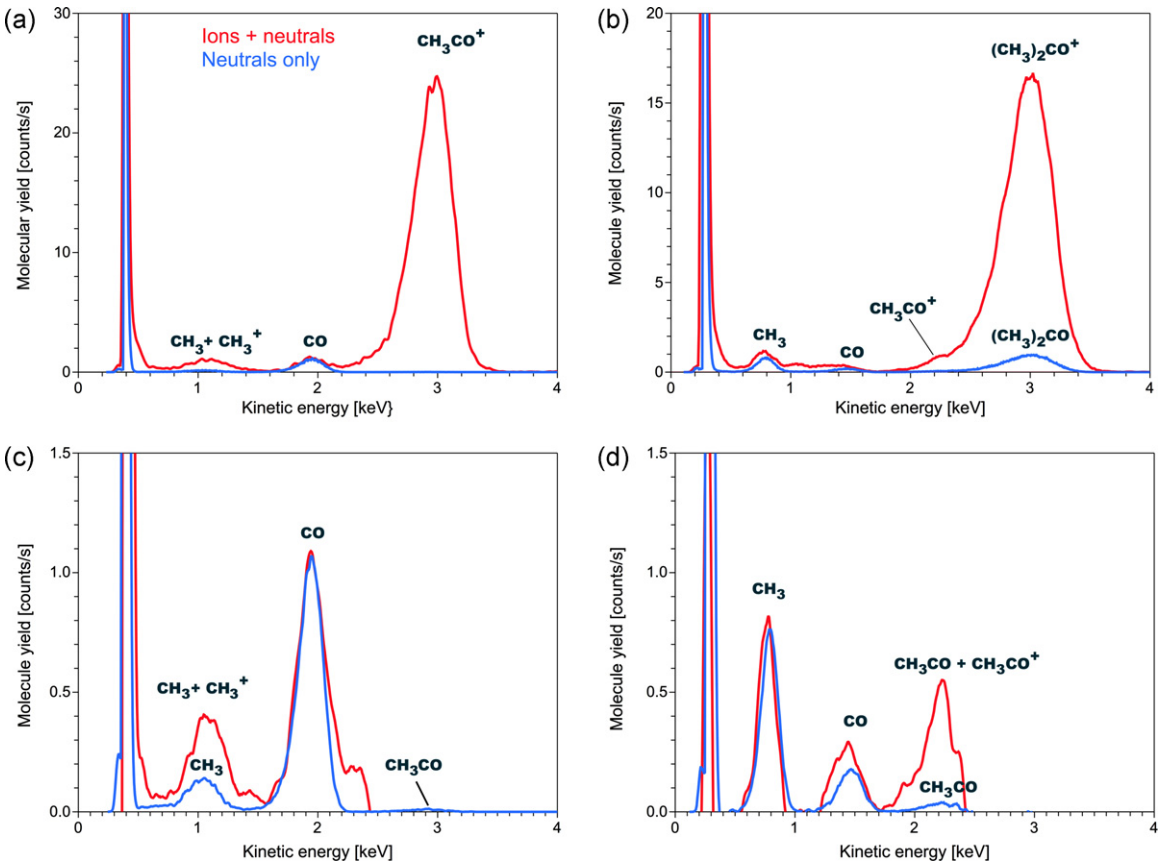

Fig. 4. Raw and processed tandem MS/KEMS spectra. (a) Raw data for acetyl precursor, CH_3CO^+. (b) Raw data for acetone precursor, $(CH_3)_2CO^+$. Blue and red curves were measured with and without activating the ion deflector, respectively. (c) Processed data for acetyl precursor. The precursor ion signal of the acetyl ions was subtracted. (d) Processed data for acetone precursor. The precursor ion signal of the acetone radical ions and the signal of the neutralized acetone molecules were subtracted.

energy difference has a higher event probability at the present collision energy, which is far below the maximum electronic transition probability based on Massey's adiabatic criteria [15,41].

To eliminate the strong precursor signals and to analyze the dissociated fragments more precisely, the spectra measured without the target gas were subtracted from the raw KEMS spectra in Fig. 4(a) and (b); the results are shown in Fig. 4(c) and (d). In addition, using the detector response function for acetone ions, the signal of the neutralized acetone molecules in Fig. 4(d) was also subtracted. The dissociated fragments are clearly separated on the kinetic energy axis. The peaks are assigned to CH_3CO^+, CH_3CO, CO, CH_3^+, and CH_3.

A striking feature of the MS/KEMS spectra is the large peak of neutral CO in Fig. 4(c), which is completely missing in conventional MS/MS data. It is recognized that the peaks of CO and CH_3 in Fig. 4(c) and (d), respectively, contain only neutrals within the accuracy of the present experiment, whereas the peaks of CH_3 and CH_3CO in Fig. 4(c) and (d), respectively, contain high fractions of the respective product ions. The CO peaks in Fig. 4(d) seem to show there are CO ions, but this may be an error when the residual artifact peak was subtracted because of the overlap between the CO and the residual artifact peak.

The observed neutral fractions indicate that the major dissociation channels are $CH_3CO^+ \rightarrow CH_3^+ + CO$ (CAD) and $CH_3CO^+ + Xe \rightarrow CH_3^\bullet + CO + Xe^+$ (ETD) for the acetyl precursor, and $(CH_3)_2CO^{+\bullet} \rightarrow CH_3CO^+ + CH_3$ (CAD), $(CH_3)_2CO^+ + Xe \rightarrow CH_3^\bullet + CH_3^\bullet + CO + Xe^+$ (ETD), and $(CH_3)_2CO^{+\bullet} + Xe \rightarrow CH_3CO + CH_3^\bullet + Xe^+$ (ETD) for the acetone precursor.

4. Discussion

The dissociation of acetone molecules has been extensively studied at low center-of-mass collision energies (E_{cm}) at 1–60 eV (e.g. [42]). CAD of acetone cations occurs primarily from electronically excited states that are isolated from the ground state, which is valid even in the present collision energy range of 3 keV [43]. Dissociation from the long-lived electronic states cannot be treated within the widely used framework of the quasi-equilibrium theory (QET) for dissociation [44]. The energy levels of the discrete electronic excitation states, which are designated as A, B, C,. . ., can be obtained from tables in Ref. [45] or other optical spectroscopic data. Compared with acetone, there is very limited information available about the electronic excitations of acetyl molecules [46]. It is expected from our following results that the lifetime of the electronic excitation states of acetyl molecules is also lengthy, however, shorter than that of acetone. We used the yield of the neutralized precursors, which survives at the detector position, the yield of the products, and a flight time of 9 μs between the collision cell and the detector to obtain the initial yields of the excited precursor neutrals. The dissociative time constants are estimated to be ~3 μs for $CH_3CO(A)^\bullet$ and ~80 μs for $(CH_3)_2CO(A)$, provided that all the surviving neutralized molecules are in the A states. The difference in the dissociative time constants is consistent with the fact that CH_3CO^+ ion and $(CH_3)_2CO$ neutral are stable, while the radicals of $CH_3CO^\bullet$ and $(CH_3)_2CO^{+\bullet}$ are unstable. In addition, the longer time constant of acetone is also consistent with the greater freedom for the dissociation channels in the neutral acetone than in the acetyl radical.

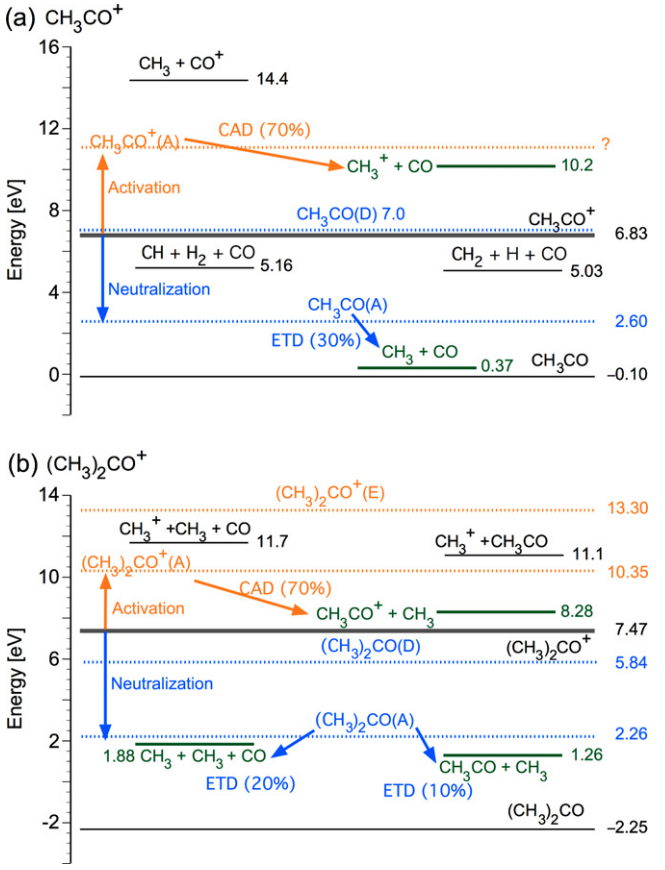

Fig. 5. Diagram of heats of formation. (a) The acetyl precursor, CH_3CO^+. (b) The acetone precursor, $(CH_3)_2CO^+$. Molecules in the diagram are categorized as the precursors (black letters), electronically excited precursor ions (orange letters), electronically excited precursor neutrals (blue letters), identified products (green letters), and unidentified products (black letters). Energy levels are indicated by the solid lines for the ground states and by the dotted lines for the electronically excited states. The reaction channels are illustrated by the orange arrows for CAD and by the blue arrows for ETD.

The thermochemical energetic diagram is shown in Fig. 5, together with the reaction efficiencies and the dissociation branching ratios. The energy levels were taken from the literature: $CH_3CO^\bullet$ and CH_3CO^+ [47], $CH_3CO(A)^\bullet$ and $CH_3CO(D)^\bullet$ [48], $(CH_3)_2CO(A)$ and $(CH_3)_2CO(D)$ [46], $(CH_3)_2CO(A)^{+\bullet}$ and $(CH_3)_2CO(E)^{+\bullet}$ [49]. The other levels were obtained from Ref. [50]. Excitations to the higher electronic states (B–E, ...) are possible, but we expect those fractions to be small. Major possible reaction channels expected from Fig. 4 are listed below with the dissociative branching ratios obtained in this study. The numbers followed by % indicate the efficiencies of the reactions relative to the precursor ion yields for the reactions (3), (5), (8), and (11) and the dissociation branching ratios obtained from the current experiment for the dissociations (6), (7), (12)–(14). The labels "CAD" and "ETD" depict the respective dissociation paths. The enthalpy differences were mostly calculated on the basis of the ground states except those marked by "A," for which ΔH values were calculated by taking into account the A state energy levels. The energy level of CH_3CO^+ (A) is unknown, but it should be between 10.2 and 14.4 eV because no CO^+ products are detectable in the acetyl precursor. It is energetically reasonable that reactions with large threshold energies (4), (9), and (10) are unobservable.

Threshold energies of acetyl reactions

$$CH_3CO^+ \rightarrow CH_3^+ + CO(CAD) \quad 4\% \quad \Delta H = 3.37\,eV \tag{3}$$

$$CH_3CO^+ \rightarrow CH_3^\bullet + CO^+(CAD) \quad \text{unidentified} \quad \Delta H = 7.57\,eV \tag{4}$$

$$CH_3CO^+ + Xe \rightarrow CH_3CO^\bullet + Xe^+(ETD) \quad 1\% \quad \Delta H = 5.20\,eV \tag{5}$$

Identified dissociation channels for acetyl

$$CH_3CO^+(A) \rightarrow CH_3^+ + CO(CAD) \quad 70\% \quad \Delta H = 0 \text{ to} -4.20\,eV \tag{6}$$

$$CH_3CO(A)^\bullet \rightarrow CH_3^\bullet + CO(ETD) \quad 30\% \quad \Delta H = -2.13\,eV \tag{7}$$

Threshold energies of acetone reactions

$$(CH_3)_2CO^{+\bullet} \rightarrow CH_3CO^+ + CH_3^\bullet(CAD) \quad 2\% \quad \Delta H = 0.81\,eV \tag{8}$$

$$(CH_3)_2CO^{+\bullet} \rightarrow CH_3CO^\bullet + CH_3^+ \quad (CAD) \quad \text{unidentified} \quad \Delta H = 3.63\,eV \tag{9}$$

$$(CH_3)_2CO^{+\bullet} \rightarrow CH_3^+ + CH_3^\bullet + CO(CAD) \quad \text{unidentified} \quad \Delta H = 4.23\,eV \tag{10}$$

$$(CH_3)_2CO^{+\bullet} + Xe \rightarrow (CH_3)_2CO + Xe^+ \quad (ETD) \quad 6\% \quad \Delta H = 2.41\,eV \tag{11}$$

Identified dissociation channels for acetone

$$(CH_3)_2CO(A)^{+\bullet} \rightarrow CH_3CO^+ + CH_3^\bullet(CAD) \quad 70\% \quad \Delta H = -2.07\,eV \tag{12}$$

$$(CH_3)_2CO(A) \rightarrow CH_3CO^\bullet + CH_3^\bullet(ETD) \quad 10\% \quad \Delta H = -1.00\,eV \tag{13}$$

$$(CH_3)_2CO(A) \rightarrow CH_3^\bullet + CH_3^\bullet + CO(ETD) \quad 20\% \quad \Delta H = -0.38\,eV \tag{14}$$

Concerning the acetyl precursor, the yield ratio of CH_3^+:$CH_3^\bullet$ = 7:3 in Fig. 5(a) indicates that the branching ratio of dissociations (6):(7) is 7:3. The ratio of CH_3CO^+:$CH_3CO^\bullet$:CO = 7:1:2 in Fig. 5(b) corresponds to that of dissociations (12):(13):(14). It has been assumed that the dominant channel for acetone is solely reaction (12), and the branching ratios of other minor channels identified are less than a few percent [46]. In reality, the present MS/KEMS data has revealed that the reaction channels involving only the product neutrals have a considerably high branching ratio of 30% for the dissociation channels (13) and (14). Moreover, it is also emphasized that the branching ratio between reactions (8) and (11) is 1:3, which means that the most dominant reaction for the acetone precursor with the Xe target is the neutralization of reaction (11). Most of the neutralized acetone molecules survive without dissociation, as seen in Fig. 4(b).

The present quantitative data on neutral fragments of acetyl and acetone are consistent with qualitative data reported using conventional MS and reionization-assisted MS. The MS/KEMS quantitative data have revealed that the reactions producing only the neutral products have considerably high branching ratios. The accuracy of branching ratio determination has to be improved in the future.

5. Conclusions

We have demonstrated that the tandem MS/KEMS with the cryodetector is effective for quantitatively identifying gas phase reaction and dissociation paths, including the cases where only multiple neutral fragments are produced, and for determining the branching ratios even when both CAD and ETD competitively occur. Such analysis has never been reported using any instruments that use the molecule detectors operating at room temperature. Our new approach is one of the ways to compensate for the neutral loss and to completely promote understanding of the gas phase ion reactions.

The high production rate of the dissociated neutral radical of $CH_3^\bullet$ may play an important role in the formation of ethyl cyanide,

methyl formate, and other prebiotic molecules in the interstellar space. It is also frequently suggested that neutral companion products have crucial structural information in fields such as glycobiology, agricultural chemistry, and cluster science. The analysis method of this work may be effective for DR experiments with compact electrostatic storage rings. The direct mass analysis of neutral molecules will contribute to ionic or molecular reactions in many areas ranging from physical chemistry to biology.

Acknowledgements

The authors are grateful to K. Suzuki, K. Chiba, N. Zen, K. Takahashi, T. Nakanaga, H. Nagai for device fabrication and the fruitful discussion. They also thank H. Akinaga and R. Maeda for their continuous fabrication support at the AIST Nanoprocessing facility and the AIST MEMS processing facility, and Y. Sato for his assistance with the MS/KEMS experiment. The part of this work was supported by the Japan Science and Technology Agency program, JST-SENTAN, and the Grant-in-Aid for Scientific Research (A) No. 22246056.

References

[1] N.G. Adams, V. Poterya, L.M. Babcock, Electron molecular ion recombination: product excitation and fragmentation, Mass Spectrom. Rev. 25 (2006) 798–828.
[2] A. Florescu-Mitchell, J. Mitchell, Dissociative recombination, Phys. Rep. 430 (2006) 277–374.
[3] L. Snyder, Interferometric observations of large biologically interesting interstellar and cometary molecules, Proc. Natl. Acad. Sci. U.S.A. 103 (2006) 12243–12248.
[4] S.A. McLuckey, T.Y. Huang, Ion/ion reactions: new chemistry for analytical MS, Anal. Chem. 81 (2009) 8669–8676.
[5] R. Zubarev, A. Zubarev, M. Savitski, Electron capture/transfer versus collisionally activated/induced dissociations: solo or duet? J. Am. Soc. Mass Spectrom. 19 (2008) 753–761.
[6] J. Sauer, M. Barrett, M. Chapman, Storage ring for neutral atoms, Phys. Rev. Lett. 87 (2001) 270401.
[7] F. McLafferty, Tandem mass-spectrometry, Science 214 (1981) 280–287.
[8] R. Thomas, When electrons meet molecular ions and what happens next: dissociative recombination from interstellar molecular clouds to internal combustion engines, Mass Spectrom. Rev. 27 (2008) 485–530.
[9] G. Angelova, O. Novotny, J. Mitchell, C. Rebrion-Rowe, J. Garrec, H. Bluhme, K. Seiersen, L. Andersen, Branching ratios for the dissociative recombination of hydrocarbon ions II. The cases of $C_4H_n^+$ (n = 1–9), Int. J. Mass Spectrom. 232 (2004) 195–203.
[10] L. Andersen, O. Heber, D. Zajfman, Physics with electrostatic rings and traps, J. Phys. B: At. Mol. Opt. Phys. 37 (2004) R57–R88.
[11] M. Ohkubo, Superconducting detectors for particles from atoms to proteins, Physica C 468 (2008) 1987–1991.
[12] G.A. Johansen, J. Stadsnes, F. Soraas, T.E. Hansen, Detection of 10–20 keV H^+, He^+ ions and electrons by planar oxide passivated and ion implanted silicon diodes, Nucl. Instrum. Methods Phys. Res. B 62 (1991) 162–166.
[14] C. Wesdemiotis, F. McLafferty, Neutralization reionization mass-spectrometry (NRMS), Chem. Rev. 87 (1987) 485–500.
[15] S. Hayakawa, Charge inversion mass spectrometry: dissociation of resonantly neutralized molecules, J. Mass. Spectrom. 39 (2004) 111–135.
[16] M. Ohkubo, M. Ukibe, S. Shiki, S. Tomita, S. Hayakawa, Direct analysis of neutrals using superconducting detector in tandem mass spectrometry, in: Presented at the 57th American Society of Mass Spectrometry (ASMS) Conference on Mass Spectrometry and Allied Topics, Philadelphia, Pennsylvania, May 2009.
[17] R.C. Dynes, V. Narayanamurti, M. Chin, Monochromatic phonon propagation in Ge:Sb using superconducting tunnel junctions, Phys. Rev. Lett. 26 (1971) 181–184.
[18] P. Lerch, A. Zehnder, Quantum Giaever detectors: STJ's, in: C. Enss (Ed.), Cryogenic Particle Detection, Springer, Berlin, 2005, pp. 217–266.
[19] D. Twerenbold, J. Vuilleumier, D. Gerber, A. Tadsen, B. Brandt, P. Gillevet, Detection of single macromolecules using a cryogenic particle detector coupled to a biopolymer mass spectrometer, Appl. Phys. Lett. 68 (1996) 3503–3505.
[20] N. Booth, Calorimetric detectors for high mass ions, Rapid Commun. Mass Spectrom. 11 (1997) 944–947.
[21] M. Frank, S. Labov, G. Westmacott, W. Benner, Energy-sensitive cryogenic detectors for high-mass biomolecule mass spectrometry, Mass Spectrom. Rev. 18 (1999) 155–186.
[22] Y. Chen, M. Ukibe, A. Kushino, M. Ohkubo, Fabrication of large array of superconducting-tunnel-junction detectors for mass spectrometry, Nucl. Instrum. Methods Phys. Res. B 559 (2006) 536–538.
[23] R. Wenzel, U. Matter, L. Schultheis, R. Zenobi, Analysis of megadalton ions using cryodetection MALDI time-of-flight mass spectrometry, Anal. Chem. 77 (2005) 4329–4337.
[24] M. Ohkubo, Y. Shigeri, T. Kinumi, N. Saito, M. Ukibe, Y. Chen, A. Kushino, A. Kurokawa, H. Sato, S. Ichimura, Fragmentation analysis by superconducting ion detectors in matrix-assisted laser desorption/ionisation (MALDI), Nucl. Instrum. Methods Phys. Res. B 559 (2006) 779–781.
[25] M. Bier, A. Ozdemir, A. Aksenov, R. Hendrix, B. Firek, The analysis of biomacromolecules using a MALDI TOF mass spectrometer incorporating a superconducting tunnel junction (STJ) cryodetector, in: Presented at the 55th American Society of Mass Spectrometry (ASMS) Conference on Mass Spectrometry and Allied Topics, Indianapolis, Indiana, June 2007.
[26] S. Shiki, M. Ukibe, Y. Sato, S. Tomita, S. Hayakawa, M. Ohkubo, Kinetic-energy-sensitive mass spectrometry for separation of different ions with the same m/z value, J. Mass Spectrom. 43 (2008) 1686–1691, Doctoral thesis (Tokyo University, 2008).
[27] G.C. Hilton, J.M. Martinis, D.A. Wollman, K.D. Irwin, L.L. Dulcle, D. Gerber, P.M. Gillevet, D. Twerenbold, Impact energy measurement in time-of-flight mass spectrometry with cryogenic microcalorimeters, Nature 391 (1998) 672–675.
[28] G. Leonard, M. Bier, An investigation of neutral and charged fragments from metastable protein ion decomposition using an energy sensitive superconducting cryodetector mass spectrometer, in: Presented at the 58th American Society of Mass Spectrometry (ASMS) Conference on Mass Spectrometry and Allied Topics, Salt Lake City, Utah, May 2010.
[29] M. Ohkubo, Superconductivity for mass spectroscopy, IEICE Trans. Electron. E90-C (2007) 550–555.
[30] S. Shiki, M. Ukibe, R. Maeda, M. Ohkubo, Y. Sato, S. Tomita, Energy resolution improvement of superconducting tunnel junction particle detectors with infrared-blocking filters, Nucl. Instrum. Methods Phys. Res. B 595 (2008) 391–394.
[31] J. Laramee, D. Cameron, R. Cooks, Collision-induced dissociation mass spectrometry: target gas effects upon scattering and charge exchange, J. Am. Chem. Soc. 103 (1982) 12–17.
[32] J. Terlouw, W. Kieskamp, J. Holmes, A. Mommers, P. Burgers, The neutralization and reionization of mass-selected positive ions by inert gas atoms, Int. J. Mass Specrom. Ion Proc. 64 (1985) 245–250.
[33] P. Danis, R. Feng, F. McLafferty, Neutralization agents for neutralization–reionization mass spectrometry, Anal. Chem. 58 (1986) 348–354.
[34] K. Qian, A. Shukla, S. Howard, S. Anderson, J. Futrell, Observation of high-energy backward scattered ions in a beam study of threshold energy collision-induced dissociation—dynamics of a long-lived excited-state of the acetone molecular ion, J. Phys. Chem. 93 (1989) 3889–3892.
[35] S. Fenistein, J. Futrell, M. Heninger, R. Marx, G. Mauclaire, Y. Yang, On the lifetime of electronically excited acetone molecular-ions, Chem. Phys. Lett. 179 (1991) 125–130.
[36] C.J. Reid, Angular scattering and internal energy deposition in kiloelectronvolt collision activated decomposition reactions of some low mass cations, Int. J. Mass Spectrom. Ion Processes 105 (1991) 191–213.
[37] N. Booth, D. Goldie, Superconducting particle detectors, Supercond. Sci. Technol. 9 (1996) 493–516.
[38] A.G. Kozorezov, A.F. Volkov, J.K. Wigmore, A. Peacock, A. Poelaert, R. Hartog, Quasiparticle-phonon down conversion in nonequilibrium superconductors, Phys. Rev. B 61 (2000) 11807–11819.
[39] M. Tinkham, Introduction to Superconductivity, 2nd ed., McGraw-Hill, New York, 1996.
[40] H. Pressler, M. Ohkubo, M. Koike, T. Zama, D. Fukuda, N. Kobayashi, Spatially resolved study of superconducting tunnel junctions X-ray detectors by low temperature scanning synchrotron microscopy, IEEE Trans. Appl. Super. 11 (2001) 696–699.
[41] H. Massey, Collisions between atoms and molecules at ordinary temperatures, Rep. Prog. Phys. 12 (1949) 248–269.
[42] R. Martinez, B. Ganguli, Kinetics and mechanism of the collision-activated dissociation of the acetone cation, J. Am. Soc. Mass Spectrom. 3 (1992) 427–444.
[43] A. Shukla, K. Qian, S. Anderson, J. Futrell, Fundamentals of tandem mass-spectrometry—a dynamics study of simple C–C bond-cleavage in collision-activated dissociation of polyatomic ions at low-energy, J. Am. Soc. Mass Spectrom. 1 (1990) 6–15.
[44] H. Resenstock, M. Wallenstein, A. Wahrhaftig, H. Eyring, Absolute rate theory for isolated systems and the mass spectra of polyatomic molecules, Proc. Natl. Acad. Sci. U.S.A. 38 (1952) 667–678.
[45] G. Herzberg, Molecular Spectra and Molecular Structure. III. Electronic Spectra and Electronic Structure of Polyatomic Molecules, Krieger Pub, Florida, 1991.
[46] R. Martinez, B. Ganguli, Instrument-independent database for collisionally activated dissociation in radiofrequency-only quadrupoles. Single-collision versus multiple-collision conditions, Rapid Commun. Mass Spectrm. 3 (1989) 427–431.
[47] J. Kercher, E. Fogleman, H. Koizumi, B. Sztaray, T.J. Baer, Heats of formation of the propionyl ion and radical and 2,3-pentanedione by threshold photoelectron photoion coincidence spectroscopy, Phys. Chem. A 109 (2005) 939–946.
[48] W. Mao, Q. Li, F. Kong, M. Huang, Ab initio calculations of the electronic states of acetyl radical, Chem. Phys. Lett. 283 (1998) 114–118.
[49] C. Brundle, M. Robin, N. Kuebler, H. Basch, Perfluoro effect in photoelectron spectroscopy. I. Nonaromatic molecules, J. Am. Chem. Soc. 94 (1972) 1451–1465.
[50] S. Lias, J. Bartmess, J. Liebman, J. Homes, R. Levin, W. Mallard, Gas-phase ion and neutral thermochemistry, J. Phys. Chem. Ref. Data 17 (1988) 1–861.